Generalized parity-time symmetry condition for enhanced sensor telemetry

Pai-Yen Chen^{1*}, Maryam Sakhdari¹, Mehdi Hajizadegan¹, Qingsong Cui¹, Mark Ming-Cheng Cheng¹, Ramy El-Ganainy^{2,3} and Andrea Alù [©] ^{4,5,6*}

Wireless sensors based on micromachined tunable resonators are important in a variety of applications, ranging from medical diagnosis to industrial and environmental monitoring. The sensitivity of these devices is, however, often limited by their low quality (Q) factor. Here, we introduce the concept of isospectral party-time-reciprocal scaling (PTX) symmetry and show that it can be used to build a new family of radiofrequency wireless microsensors exhibiting ultrasensitive responses and ultrahigh resolution, which are well beyond the limitations of conventional passive sensors. We show theoretically, and demonstrate experimentally using microelectromechanical-based wireless pressure sensors, that PTX-symmetric electronic systems share the same eigenfrequencies as their parity-time (PT)-symmetric counterparts, but crucially have different circuit profiles and eigenmodes. This simplifies the electronic circuit design and enables further enhancements to the extrinsic Q-factor of the sensors.

he wireless monitoring of physical, chemical and biological quantities is essential in a range of medical and industrial applications in which physical access and wired connections would introduce significant limitations. Examples include sensors that are required to operate in harsh environments, and those that are embedded in, or operate in the vicinity of, human bodies¹. Telemetric sensing based on compact, battery-less wireless sensors is one of the most feasible ways to perform contactless continuous measurements in such applications. The first compact passive wireless sensor was proposed in 1967², and used a miniature spiral inductor (L) and a pressure-sensitive capacitor (C) to build a resonant sensor that could measure the fluid pressure inside the eye (an intraocular pressure sensor). The idea was based on a mechanically adjusted capacitor (or varactor), which has been an effective way of tuning resonant circuits since the advent of the radio³. Despite this, wireless capacitive sensing technology has experienced a rapid expansion only in the last two decades, due to the development of microelectromechanical systems (MEMS), nanotechnology and wireless technology⁴⁻⁸.

Recently, low-profile wireless sensors based on passive LC oscillating circuitry (typically a series RLC tank) have been used to measure pressure^{5,6}, strain⁷, drug delivery⁸, temperature, and chemical reactions¹. The working principle of these passive LC sensors is typically based on detecting concomitant resonance frequency shifts, where the quantity to be measured detunes capacitive or inductive elements of the sensor. This could occur, for example, through mechanical deflections of electrodes, or variations of the dielectric constant. In general, the readout of wireless sensors relies on mutual inductive coupling (Fig. 1a), and the sensor information is encoded in the reflection coefficient. Such telemetric sensor systems can be modelled using a simple equivalent circuit model, in which the compact sensor is represented by a series resonant RLC tank, where the resistance R takes into account the power dissipation of the sensor (Fig. 1a).

Although there has been continuous progress in micro- and nano-machined sensors in recent years, the basics of the telemetric readout technique remain essentially unchanged since its invention. Nonetheless, improving the detection limit is often hindered by the available levels of *Q*-factor, the sensing resolution and the sensitivity related to the spectral shift of resonance in response to variations of the physical property to be measured. In particular, modern *LC* microsensors based on thin-film resonators or actuators usually have a low modal *Q*-factor, due to relevant power dissipations caused by skin effects, Eddy currents and the electrically lossy surrounding environment (such as biological tissues)⁹. A sharp, narrowband reflection dip has been a long-sought goal for inductive sensor telemetry, because it could lead to superior detection and great robustness to noises.

In this Article, we introduce a generalized parity–time (*PT*)-symmetric telemetric sensing technique, which enables new mechanisms to manipulate radiofrequency (RF) interrogation between the sensor and the reader, to boost the effective *Q*-factor and sensitivity of wireless microsensors. We implement this sensing technique using MEMS-based wireless pressure sensors operating in the RF spectrum.

Generalized PT-symmetry

The concept of *PT*-symmetry was first proposed in the context of quantum mechanics¹⁰ and has been extended to classical wave systems, such as optics^{11–13}, owing to the mathematical isomorphism between Schrodinger and Helmholtz wave equations. *PT*-symmetric optical structures with balanced gain and loss have unveiled several exotic properties and applications, including unidirectional scattering^{14,15}, coherent perfect absorber-lasers^{16,17}, single-mode micro-ring lasers^{18–20} and optical non-reciprocity^{21–24}. Inspired by optical schemes, other *PT*-symmetric systems in electronics (sub-RF, 30 kHz and below^{25–27}), acoustics²⁸ and optomechanics^{29,30} have

Department of Electrical and Computer Engineering, Wayne State University, Detroit, MI, USA. ²Department of Physics and Henes Center for Quantum Phenomena, Michigan Technological University, Houghton, MI, USA. ³Department of Electrical and Computer Engineering, Michigan Technological University, Houghton, MI, USA. ⁴Advanced Science Research Center, City University of New York, New York, NY, USA. ⁵Graduate Center of the City University of New York, New York, New York, NY, USA. ⁶Department of Electrical Engineering, City College of New York, New York, NY, USA.

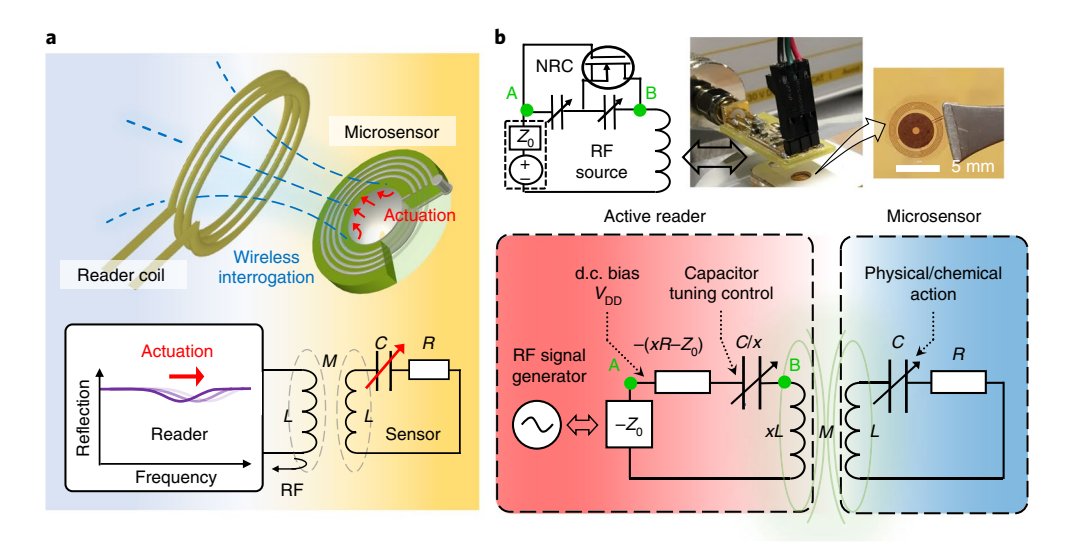


Fig. 1 | Non-Hermitian telemetric sensor system. a, Schematic diagrams of a typical wireless implantable or wearable sensor system, where a loop antenna is used to interrogate the sensor via inductive (magnetic) coupling. The parameters to be sensed can be accessed by monitoring the reflection coefficient of the sensor, typically based on an *RLC* resonant circuit consisting of a micromachined varactor and inductor. **b**, Equivalent circuit model for the proposed *PTX*-symmetric telemetric sensor system, where x is the scaling coefficient of the reciprocal-scaling operation \mathcal{X} . If x = 1, the *PTX* system converges to the *PT*-symmetric case. In the closed-loop normal mode analysis, an RF signal generator with a source impedance Z_0 , connected to the reader, is represented by $-Z_0$. The inset shows the a.c. model for the Colpitts circuit with a positive feedback, which achieves an equivalent negative resistance and an equivalent series capacitance.

also been reported recently. The exceptional points arising in these systems, found at the bifurcations of eigenfrequencies near the PT-phase transition, show the potential to enhance the sensitivity of photonic sensors^{31–35}.

In principle, exceptional points and bifurcation properties of a PT-symmetric system can be utilized also to enhance sensor telemetry, represented by the equivalent circuit in Fig. 1b with x=1. In this case, the PT-symmetry condition is achieved when the gain and loss parameters, namely -R and R, are delicately balanced, and the reactive components, L and C, satisfy mirror symmetry: that is, the impedances of the active and passive circuit tanks, multiplied by i, are complex conjugates of each other at the frequency of interest. Similar to earlier experiments in optical systems²², the realization of PT-symmetry in a telemetric sensor system is expected to exhibit real eigenfrequencies in the exact symmetry phase. This leads to sharp and deep resonances, beyond the limitations discussed above for passive systems, thus providing improved spectral resolution and modulation depth for sensing. Despite this advantage of traditional PT-symmetric systems, practical implementations for the sensor telemetry may encounter difficulties in achieving an exact conjugate impedance profile. For instance, given the limited area of medical bioimplants and MEMS-based sensors, the inductance of the sensor's microcoil L_s is usually smaller than the one of the reader's coil L_R . Although downscaling the reader coil can match L_R to L_s, this would reduce the mutually inductive coupling and degrade the operation of the wireless sensor. Therefore, it is highly desirable to have extra degrees of freedom that allow arbitrary scaling of the coil inductance and other parameters (for example, capacitance and equivalent negative resistance) in the reader, to optimize the wireless interrogation and facilitate the electronic circuit integration.

To overcome these difficulties, and at the same time significantly improve the sensing capabilities of telemetric sensors, we also introduce here the idea of PTX-symmetric telemetry (Fig. 1b). This PTX-symmetric electronic system consists of an active reader (equivalently, a -RLC tank), wirelessly interrogating a passive microsensor (RLC tank) via the inductive coupling. Here, the equivalent series -R is achieved with a Colpitts-type circuit (Fig. 1b), which acts as a negative-resistance converter (NRC) (see Supplementary

Note 1 for detailed design, analysis and characterization of the circuit). By suitably scaling the values of -R, L and C in the active reader, the system can be made invariant under the combined parity transformation $\mathcal{P}(q_1 \leftrightarrow q_2)$, time-reversal transformation $\mathcal{T}(t \to -t)$ and reciprocal scaling $\mathcal{X}(q_1 \to x^{1/2}q_1, \ q_2 \to x^{-1/2}q_2)$, where $q_1(q_2)$ corresponds to the charge stored in the capacitor in the -RLC (RLC) tank and x is the reciprocal-scaling coefficient, an arbitrary positive real number. In the following analysis, we will prove that the introduced X transformation allows the operation of a system with unequal gain and loss coefficients (also an asymmetric reactance distribution), while exhibiting an eigenspectrum that is identical to the one of the PT-symmetric system. Crucially, the scaling operation \mathcal{X} offers an additional degree of freedom in sensor and reader designs, overcoming the mentioned space limitations of microsensors that pose challenges in realizing PT-symmetric telemetry. Even more importantly, while the scaling provided by the X operator leaves the eigenspectrum unchanged, it leads to linewidth sharpening and thus boosts the extrinsic Q-factor, the sensing resolution and the overall sensitivity.

As we demonstrate below, the effective Hamiltonians of PTX and PT systems are related by a mathematical similarity transformation. We start by considering Kirchoff's law of the equivalent circuit representation of the PTX telemetric sensor system (Fig. 1b) cast in the form of a Liouville-type equation $\partial_t \Psi = \mathcal{L}\Psi$ (ref. 25) governing the dynamics of this coupled RLC/-RLC dimer, where the Liouvillian \mathcal{L} is given by

$$\mathcal{L} = \begin{pmatrix} 0 & 0 & 1 & 0 \\ 0 & 0 & 0 & 1 \\ -\frac{1}{1-\kappa^2} & \frac{1}{\sqrt{x}} \frac{\kappa}{1-\kappa^2} & \frac{1}{\gamma(1-\kappa^2)} & \frac{1}{\sqrt{x}} \frac{\kappa}{\gamma(1-\kappa^2)} \\ \sqrt{x} \frac{\kappa}{1-\kappa^2} & -\frac{1}{1-\kappa^2} & -\sqrt{x} \frac{\kappa}{\gamma(1-\kappa^2)} & -\frac{1}{\gamma(1-\kappa^2)} \end{pmatrix}$$
(1)

and $\Psi \equiv (q_1, q_2, \dot{q}_1, \dot{q}_2)^T$, $\tau \equiv \omega_0 t$, the natural frequency of an isolated lossless LC tank $\omega_0 = 1/\sqrt{LC}$, the coupling strength between the active and passive tanks $\kappa = M/\sqrt{L_R L_S}$, $L_R = xL$,

NATURE ELECTRONICS ARTICLES

 $L_S=L$ and the dimensionless non-Hermiticity parameter $\gamma=R^{-1}\sqrt{L/C}=(x|-R|)^{-1}\sqrt{(xL)/(C/x)}$; here, all frequencies are measured in units of ω_0 . The active and passive tanks have the same non-Hermiticity parameter γ , regardless of the value of x (PT or PTX system). From equation (1), we can define an effective Hamiltonian $H=i\mathcal{L}$ with non-Hermitian form (that is, $H^{\dagger}\neq H$). Such a non-Hermitian Hamiltonian system is invariant under a combined PTX transformation, with

$$\mathcal{P} = \begin{pmatrix} \sigma_x & 0 \\ 0 & \sigma_x \end{pmatrix} \tag{2a}$$

$$\mathcal{T} = \begin{pmatrix} \mathbf{1} & 0 \\ 0 & -\mathbf{1} \end{pmatrix} \mathcal{K} \tag{2b}$$

$$\mathcal{X} = \mathbf{1} \otimes x_0 \text{ and } x_0 = \begin{pmatrix} x^{1/2} & 0 \\ 0 & x^{-1/2} \end{pmatrix}$$
 (2c)

where σ_x is the Pauli matrix, $\mathbf{1}$ is the identity matrix, \mathcal{K} performs the operation of complex conjugation and $(\mathcal{P}T\mathcal{X})^2=\mathbf{1}$. The Hamiltonian and eigenmodes of the PTX system are related to those of the PT system (H', Ψ') through the similarity transformation $H=\mathcal{S}^{-1}H'$ \mathcal{S} and $\Psi=\mathcal{S}^{-1}\Psi'$, where \mathcal{S} is an invertible 4-by-4 matrix $\mathcal{S}=\mathbf{1}\otimes\zeta$ and $\zeta=\begin{pmatrix}x^{1/2}&0\\0&1\end{pmatrix}$. As a result, PTX and PT systems share the same eigenfrequencies, but possess different eigenmodes. Moreover, H commutes with the transformed operators $P=\mathcal{S}^{-1}P\mathcal{S}$ and $P=\mathcal{S}^{-1}T\mathcal{S}=\mathcal{T}$, that is, [PT,H]=0, where P performs the combined operations of parity and reciprocal scaling: $P=\mathcal{F}^{-1}P\mathcal{F}$ and, therefore, $P=\mathcal{F}^{-1}P\mathcal{F}$ commutes also with $PT\mathcal{F}$ (that is, $PT\mathcal{F}$, $PT\mathcal{F}$, and, therefore, $P=\mathcal{F}$ commutes also with $PT\mathcal{F}$ (that is, $PT\mathcal{F}$). In the limit when the scaling coefficient P, the PTX-symmetric system converges into the traditional PT-symmetric system. Hence, the PTX-symmetry can be regarded as a generalized group of the PT-symmetry.

PT/PTX-symmetric telemetric microsensor systems

We designed and realized the sensor using a micromachined parallel-plate varactor connected in series to a micromachined planar spiral inductor and also a parasitic resistance (Fig. 1b). Figure 2a-c shows schematic diagrams and a photograph of the realized device, together with its detailed surface profiles characterized by scanning white-light interferometry (SWLI) (see Supplementary Notes 1 and 2 for design and fabrication details). The sensor was encapsulated with epoxy polyamides and connected to an air compressor, and a microprocessor-controlled regulator was used to vary the internal pressure inside the MEMS microcavity from 0 mmHg to 200 mmHg. This procedure simulates, for instance, pressure variations inside the human eye6 (see Methods for the detailed measurement set-up). The sensor can be seen as a tunable passive *RLC* tank, in which the applied pressure mechanically deforms the floating electrode of the varactor (Fig. 2a), causing a change in the total capacitance. Figure 2d presents the extracted capacitance as a function of the internal pressure, with insets showing the corresponding cross-sectional SWLI images (see Supplementary Note 1 for the extraction of RLC values). The measurement results agree well with theoretical predictions, revealing that the capacitance is reduced by increasing the applied pressure.

In our first set of experiments, we designed an active reader, which, together with the passive microsensor, forms the PTsymmetric dimer circuit. We investigate the evolution of complex eigenfrequencies and reflection spectra as we vary γ and κ . In our measurements, the sensor was fixed on an XYZ linear translation stage used to precisely control κ . For a specific value of κ , γ was tuned by the equivalent capacitance of the microsensor, responsible for the applied pressure. On the reader side, the voltage-controlled impedance converter provides an equivalent negative resistance, whose magnitude is set equal to $-(R-Z_0)$, where the sensor's effective resistance R was measured to be $\sim 150 \Omega$ and Z_0 is the source impedance of the RF signal generator (for example, the vector network analyser (VNA) used in the experiment, with $Z_0 = 50 \Omega$) connected in series to the active reader. We note that, in the closed-loop analysis, an external RF source can be modelled as a negative resistance $-Z_0$, as it supplies energy to the system³. When the sensor's capacitance changed, the voltage-controlled varactor in the reader

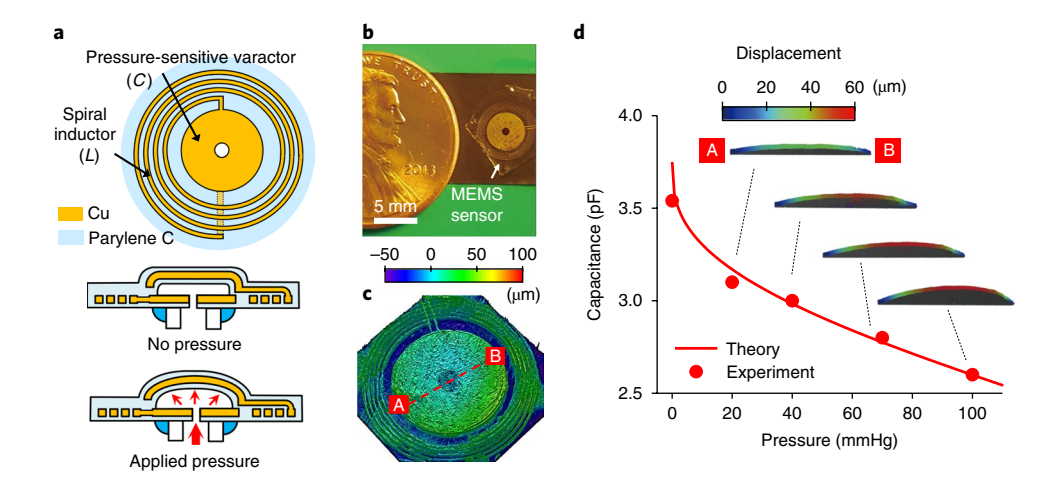


Fig. 2 | MEMS-based wireless pressure sensor. a, Schematic diagrams of a MEMS-based pressure sensor, which consists of a variable parallel-plate capacitor (*C*) connected in series with a microcoil inductor (*L*), effectively forming a resonant *LC* tank circuit. Increasing the internal pressure by using an air compressor regulator increases the displacement of the upper membrane electrode, thereby reducing the capacitance of the MEMS varactor. **b**, Top view of the microfabricated wireless pressure sensor on a flexible polymer substrate. **c**, Three-dimensional surface profile of the sensor in **b**, which was measured by SWLI. **d**, Measurement (dots) and theoretical (solid line) results for the total capacitance in response to pressure (Supplementary Note 1); the insets show the displacement of the upper membrane electrode measured by SWLI. Due to the cylindrical symmetry of the capacitor, only displacements in the radial direction (from point A to point B in **c**) are shown.

circuit was adjusted accordingly to maintain the PT-symmetry condition (see Supplementary Note 1 for details of reader design). Wireless pressure sensing was performed by monitoring in situ the shift of resonance in the reflection spectrum across 100-350 MHz. In our measurements, a clear eigenfrequency bifurcation with respect to γ and κ of the PT-symmetric system was observed (as shown in Fig. 3a) and the agreement between experimental results (dots) and theory (coloured contours) is excellent; a detailed theoretical analysis of the critical points is provided in the Methods. At the exceptional point γ_{EP} , real eigenfrequencies branch out into the complex plane. In the region of interest $\gamma \in [\gamma_{EP}, \infty]$, the eigenfrequencies are purely real ($\omega \in \mathbb{R}$) (Fig. 3a) and $\mathcal{P}T\Psi' = \Psi'$, such that the PT-symmetry condition is exactly met in the so-called exact PTsymmetric phase. In this phase, the oscillation occurs at two distinct eigenfrequencies corresponding to sharp reflection dips (Fig. 3c). Before passing γ_{EP} , the system is in its broken *PT*-symmetric phase, where complex eigenfrequencies ($\omega \in \mathbb{C}$) exist in the form of complex conjugate pairs, and the PT-symmetry of eigenmodes is broken, namely $PT\Psi' \neq \Psi'$. The system exhibits a phase transition when the non-Hermiticity parameter exceeds the critical value γ_{EP} , at which point the non-Hermitian degeneracy can unveil several counterintuitive features, such as the unidirectional reflectionless transparency^{14,28} and the singularity-enhanced sensing^{31–35}.

To better illustrate the system response, we plot the measured reflection spectra, where γ is fixed to 2.26 (corresponding to an applied pressure of 100 mmHg), while κ is continuously varied from 0.4 to 0.5 (Fig. 3c). The evolution of the resonant response clearly identifies the eigenfrequency transition (Fig. 3a). In the weak coupling region, the system operates in the broken PT-symmetric phase, quantified by $\kappa < \kappa_{PT}$, and its complex eigenfrequency results in a weak and broad resonance. This can be explained by the fact that, if the coupling strength is weak, the energy in the active –*RLC* tank cannot flow fast enough into the passive RLC tank to compensate for the absorption, thereby resulting in a non-equilibrium system with complex eigenfrequencies. If the coupling strength exceeds a certain threshold, the system can reach equilibrium, since the energy in the active tank can flow fast enough into the passive one to compensate its power dissipation. From Fig. 3a, we observe that at higher κ , the threshold of γ for the phase transition (γ_{EP}) can be reduced. As a result, a PT-symmetric telemetric sensor system, if designed properly to work in the exact PT-symmetric phase quantified by $\kappa > \kappa_{PT}$, can exhibit sharp and deep resonant reflection dips, ensuring high sensitivity with electrical noise immunity. From the circuit viewpoint, the reflectionless property in the one-port measurement is due to impedance matching. In the exact PT-symmetric phase with real eigenfrequencies, the input impedance looking into the active reader can be matched to the generator impedance Z_0 at the eigenfrequencies (or resonance frequencies), leading to the dips observed in the reflection spectrum.

We also note that the splitting of the Riemann surface outlined in Fig. 3a may lead to an interesting topological response, implying a dramatic shift of the resonance frequency when γ is altered by pressure-induced capacitance changes in the microsensor ($\gamma \propto C^{-1/2}$). It is interesting to compare these results with those obtained with a conventional fully passive telemetric sensing scheme (Fig. 3b)⁴⁻⁹, where the negative-resistance converter and varactors are removed from the active reader, leaving a coil antenna to interrogate the same pressure sensor. In this case, the eigenfrequency of the conventional passive system is always complex (Fig. 3b), no matter how γ and κ are varied, as expected for a lossy resonator, and the eigenfrequency surface is rather flat for both real and imaginary parts when compared with the PT-symmetric system (Fig. 3a). Figure 4a,b presents the evolution of the reflection spectra for the two sensing systems; here, κ is fixed to 0.5 and γ is varied by changing the applied pressure (20, 40, 70 and 100 mmHg). The bifurcation of eigenfrequency in the PT-symmetric system (Fig. 4b) leads to the formation of two

eigenmodes with sharp reflection dips, whose spectral shifts in response to γ can be dramatic and coincides with the topological phase transition shown in Fig. 3a. On the other hand, the passive system (Fig. 4a) exhibits a broad resonance, associated with a low sensing resolution, and a less observable change in the resonance frequency. It is evident that a PT-symmetric telemetric sensor can provide largely superior sensitivity when compared with conventional passive ones⁴⁻⁹, as it achieves not only a finer spectral resolution in light of a higher Q-factor, but also more sensitive frequency responses (Fig. 5a).

Next, we explore the functionality of the PTX-symmetric sensor within the same telemetry platform. Unlike the PT-symmetric system, the reciprocal scaling in the PTX system breaks the mirror symmetry of the effective $|\pm R|$, L and C; namely, their values in the sensor and the reader can be quite different for large or small values of x. In our experiments, the same MEMS-based pressure sensor was now paired with a new type of reader (Fig. 1b), whose equivalent circuit is similar to the reader used in Fig. 4b, but with all elements scaled following the rule: $-R \rightarrow -xR$, $L \rightarrow xL$ and $C \rightarrow x^{-1}C$. This realizes a PTX-symmetric telemetry system that has a non-Hermitian Hamiltonian H (equation (1)) commuting with $\mathcal{P}T\mathcal{X}$ (equation (2)). We have tested different values of x to investigate its effect on eigenfrequencies; here, κ was fixed to 0.5 in different set-ups. Figure 5a shows the real and imaginary parts of eigenfrequencies against γ for PTX-symmetric telemetric sensor systems with x=3, 1/3 and 1. We note that x=1 corresponds to the PT-symmetric system discussed before.

We observe that a non-Hermitian *PTX*-symmetric Hamiltonian also supports real eigenfrequencies in the exact PTX-symmetric phase, thus leading to sharp and deep resonant reflection dips. As discussed earlier, in spite of the introduction of the \mathcal{X} operator, the PTX-symmetric system and its PT-symmetric counterpart possess exactly the same eigenspectrum and bifurcation points, as clearly seen in Fig. 5a. In the PTX system, there is also a clear transition between the exact PTX-symmetric phase $(\mathcal{P}T\mathcal{X}\Psi=\Psi)$ and the broken PTX-symmetric phase $(\mathcal{P}T\mathcal{X}\Psi\neq\Psi)$, which are respectively characterized by real and complex eigenfrequencies. The theoretical and experimental results in Fig. 5a imply that the spectral shift of resonance associated with the exceptional-point singularity in a PT-symmetric sensor can be likewise obtained in a PTX-symmetric sensor, as the same eigenspectrum is shared. We note that the PT and PTX systems, although sharing the same eigenspectrum, can have different eigenmodes; that is, $\Psi = S^{-1}\Psi'$ and S is correlated with x. Figure 5b presents reflection spectra for the PTX-symmetric telemetric sensor with x=3, under different applied pressures. Due to the scaling operation \mathcal{X} in the PTX-symmetric system, it is possible to further reduce the linewidth of the reflection dip and achieve a finer sensing resolution by increasing the value of x. In contrast to the case x > 1, x < 1 results in broadening of the resonance linewidth and thus a lowered Q-factor. We note that the input impedance (looking into the active reader) of PT- and PTX-symmetric telemetry systems can be identical and matched to the generator impedance Z₀ at their shared resonance frequencies, corresponding to reflectionless points (see Supplementary Note 3). As the frequency is away from the resonance frequency, the input impedance and reflection coefficient of PT- and PTX-symmetric systems may be very different, leading to a different resonance linewidth as a function of x. As a result, the PTX-symmetric telemetric sensor system (Fig. 5b), when compared with the *PT*-symmetric one (Fig. 4b), not only offers more design flexibility by removing certain physical constraints (for example, mirror-symmetric $|\pm R|$, L and C in the mutually coupled circuit), but also could support greater resolution, sensitivity and potentially longer interrogation distance enabled by the optimally designed self and mutual inductances of coils. Most importantly, both systems exhibit the same eigenspectrum and exceptional point. Ideally, in the exact PTX-symmetry phase, there

NATURE ELECTRONICS ARTICLES

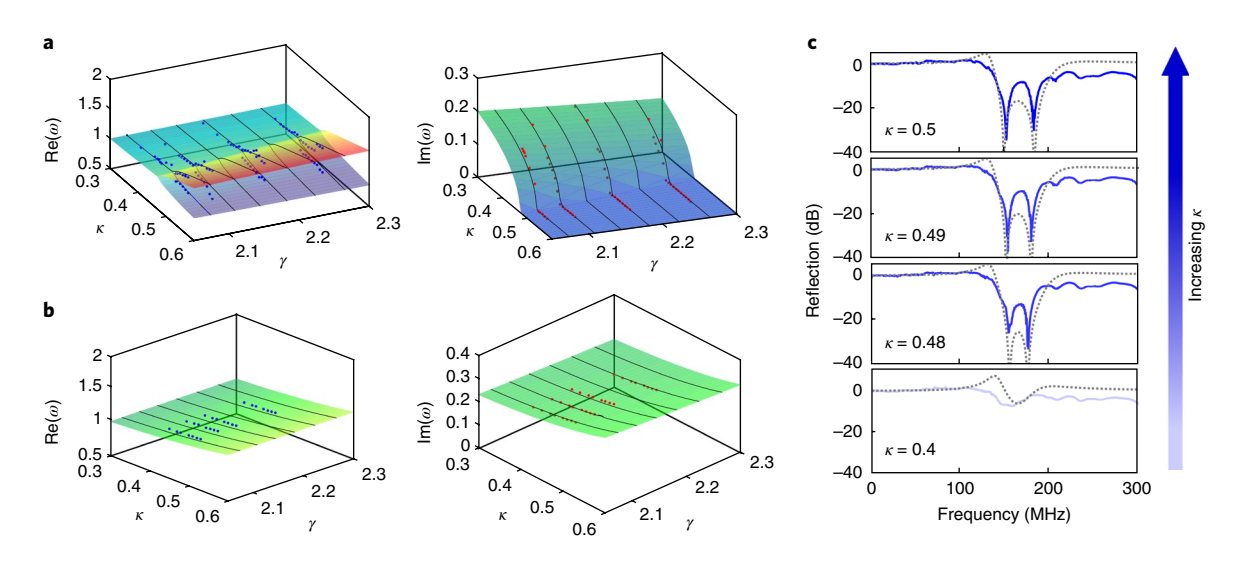


Fig. 3 | **Evolution of eigenfrequencies and reflection spectra as a function of the non-Hermiticity parameter \gamma and coupling strength \kappa. a,b, Real (a, left) and imaginary (a, right) eigenfrequency isosurface normalized by \omega_0 in the (\gamma,\kappa) parameter space for a** *PT***-symmetric wireless pressure sensor and a conventional passive wireless pressure sensor (b), where an active reader and a passive loop antenna are respectively used to interrogate the micromachined sensor in Fig. 2. c**, Reflection spectra against the frequency for the *PT*-symmetric wireless pressure sensor with different coupling strengths, showing a transition from the broken *PT*-symmetric phase (κ = 0.4) to the exact *PT*-symmetric phase (κ = 0.48, 0.49 and 0.5) when κ increases; here γ = 2.26, corresponding to an applied pressure of 100 mmHg, and $\omega_0/2\pi$ = 180 MHz. The frequencies and linewidths of the reflection dips in **c** are consistent with the eigenfrequency evolution in **a**. The solid and dashed lines denote experimental data and theoretical results obtained from the equivalent circuit model in Fig. 1.

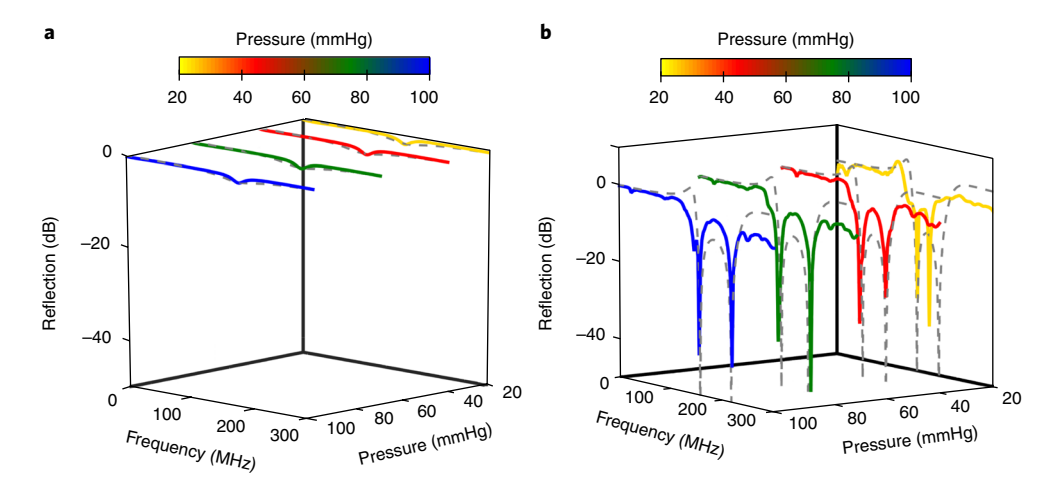


Fig. 4 | Pressure-induced spectral changes for conventional and *PT***-symmetric telemetric sensors. a,b**, The magnitude of the reflection coefficient for the MEMS-based pressure sensor (Fig. 2) interrogated by the conventional passive loop antenna (a) and the active reader realizing a *PT*-symmetric dimer (b), under different applied pressures. The solid and dashed lines denote experimental data and theoretical results obtained from the equivalent circuit models.

is no fundamental limit to the Q-factor enhancement. In the extreme case when x approaches infinity, the resonance linewidth becomes infinitesimally narrow, namely the Q-factor is close to infinity, provided that such a reader circuit can be realized. However, in reality, the -R, L and C values of electronic devices have their own limits.

For generality, a microsensor (negative-resistance converter) can in principle be decomposed into a series or parallel equivalent RLC (-RLC) tank, and either choice is formally arbitrary, depending on the sensor and circuit architectures and on the kind of excitation (that is, impressed voltage or current source). The concept of PTX-symmetry can also be generalized to an electronic dimer utilizing the parallel circuit configuration, whose PT-symmetric counterpart has been demonstrated^{25,26}. It may also be possible to enhance the performance and resolution of a wireless resonant

sensor modelled by a parallel RLC tank if the sensor is interrogated by a parallel -RLC tank^{25,26}, to satisfy the PTX-symmetry condition (see Supplementary Note 3 for an example of the PTX-symmetric parallel circuit).

It is important to note that, in the exact symmetry phase of the PTX-symmetric system, although the gain and loss parameters (-xR and R) are not equal, the net power gained in the active tank and the one dissipated in the passive tank are balanced, similar to the PT-symmetric case. In the closed-loop analysis, the power loss in the passive tank $P_{\rm loss} = |\dot{\mathbf{q}}_1|^2 R/2$, while the power gained in the active tank $P_{\rm gain} = |\dot{\mathbf{q}}_1|^2 (xR-Z_0)/2 + |\dot{\mathbf{q}}_1|^2 Z_0/2$ (where the first term accounts for power gained from the negative-resistance device and the second term corresponds to the external energy source modelled as a negative resistance $-Z_0$). Since the PTX-symmetry

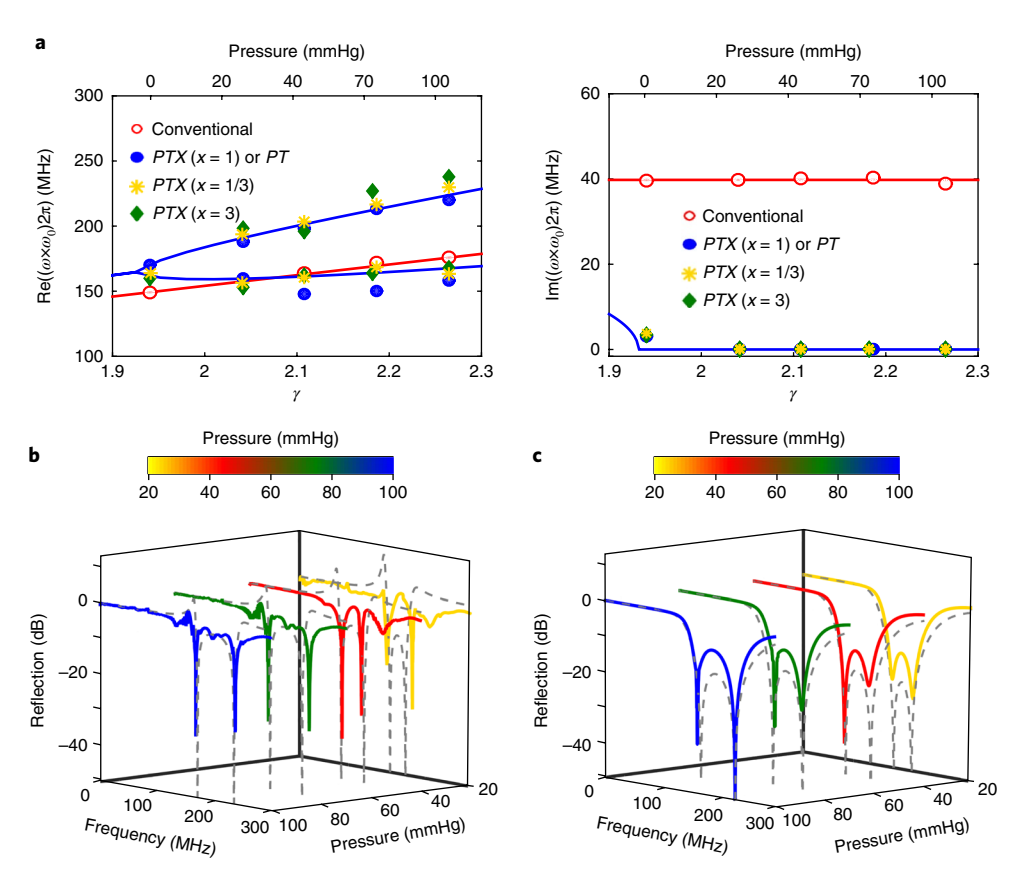


Fig. 5 | Evolution of the eigenfrequencies and reflection spectra for *PTX***-symmetric telemetric sensors. a**, Real (left) and imaginary (right) eigenfrequency as a function of the non-Hermiticity parameter γ for the fully passive (red open circles; Fig. 4a), *PT*-symmetric (blue dots; Fig. 4b) and *PTX*-symmetric (green and yellow symbols; **b** and **c**) telemetric pressure sensors. The solid lines denote theoretical predictions (see Methods). **b,c**, The magnitude of the reflection coefficient for the *PTX*-symmetric telemetric sensor systems; here, the scaling coefficients x used in **b** and **c** are 3 and 1/3. The solid and dashed lines in **b** and **c** denote the experimetrial data and theoretical predictions.

enforces the condition $\dot{\mathbf{q}}_1 = \dot{\mathbf{q}}_2/\sqrt{x}$, gain and dissipation are always balanced in this system (that is, $P_{\rm gain} = P_{\rm loss}$), regardless of the value of x. Therefore, although this generalized PT-symmetric system allows for arbitrary scaling of the gain and loss parameters (-R and R here), the gain–loss power balance is maintained in the exact symmetry condition, as expected by the fact that the eigenvalues are real. However, greater design flexibility on the linewidth of the response could be enabled.

Finally, it is interesting to note that in the PTX-symmetric system, if x is sufficiently small such that $xR-Z_0 \le 0$, both the reader and sensor circuits can be fully passive; namely, an inductively coupled RLC/RLC dimer is used. Such an observation is in stark contrast with what one would expect in conventional PT-symmetric systems, where pertinent gain or amplification is necessary to enable the associated peculiar phenomena. Figure 5c presents reflection spectra for the PTX-symmetric telemetric sensor system with x = 1/3; in this case, the reader is also a passive RLC tank without the need of a negative-resistance or amplification device. We observe a broad resonance, as the linewidth of the reflection dip is widened by decreasing the value of x. This operating regime (x=1/3), although not necessarily of interest for enhanced sensing capabilities, provides an interesting platform to study the dynamics of exceptional points and non-Hermitian physics in a loss-loss dimer, without the need for any active component. The presented PTX-symmetric dimer structure may also be extended to other frequencies, including light and ultrasonic waves. For instance, one potential application of our proposed reciprocally scaling operation is to provide an additional knob to tailor the threshold gain of PT-symmetric single-mode lasers^{18–20} or coherent perfect absorberlasers^{16,17} by breaking the exact balance of gain and loss coefficients, while preserving the spectrum of eigenvalues.

Conclusions

We have applied PT-symmetry and the generalized PTX-symmetry introduced here to RF sensor telemetry, with a particular focus on compact wireless micro-mechatronic sensors and actuators. Our approach overcomes the long-standing challenge of implementing a miniature wireless microsensor with high spectral resolution and high sensitivity, and opens opportunities to develop loss-immune high-performance sensors, due to gain-loss interactions via inductive coupling and eigenfrequency bifurcation resulting from the PT (PTX)-symmetry. Our findings also provide alternative schemes and techniques to reverse the effects of loss and enhance the Q-factor of various RF systems. Through our study of PTXsymmetry, we have shown that even asymmetric profiles of gain and loss coefficients can yield exotic non-Hermitian physics observed in PT-symmetric structures. Importantly, compared to PT-symmetry, PTX-symmetry offers greater design flexibility in manipulating resonance linewidths and Q-factors, while exhibiting eigenfrequencies identical to the associated *PT*-symmetric system.

Methods

Exceptional point and phase transitions. Applying Kirchhoff's laws to the *PTX*-symmetric circuit in Fig. 1b leads to the following set of equations:

$$\frac{d^{2}q_{1}}{d\tau^{2}} = -\frac{1}{1-\kappa^{2}}q_{1} + \frac{1}{\sqrt{x}}\frac{\kappa}{1-\kappa^{2}}q_{2} + \frac{1}{\gamma(1-\kappa^{2})}\dot{q}_{1} + \frac{1}{\sqrt{x}}\frac{\kappa}{\gamma(1-\kappa^{2})}\dot{q}_{2}$$
(3a)

NATURE ELECTRONICS ARTICLES

$$\frac{\mathrm{d}^{2}q_{2}}{\mathrm{d}\tau^{2}} = \sqrt{x} \frac{\kappa}{1 - \kappa^{2}} q_{1} - \frac{1}{1 - \kappa^{2}} q_{2} - \sqrt{x} \frac{\kappa}{\gamma (1 - \kappa^{2})} \dot{q}_{1} - \frac{1}{\gamma (1 - \kappa^{2})} \dot{q}_{2} \tag{3b}$$

which leads to the Liouvillian formalism in equation (1). After the substitution of time-harmonic charge distributions $q_n = A_n e^{i o \tau}$, eigenfrequencies and normal modes for this PTX-symmetric electronic circuit can be computed from the eigenvalue equation $(H-\omega_k 1)\Psi_k = 0$, with k=1,2,3,4. The eigenfrequencies associated with the non-Hermiticity parameter γ and coupling strength κ can be derived as:

$$\omega_{1,2,3,4} = \pm \sqrt{\frac{2\gamma^2 - 1 \pm \sqrt{1 - 4\gamma^2 + 4\gamma^4 \kappa^2}}{2\gamma^2 (1 - \kappa^2)}}$$
 (4)

There is a redundancy in equation (4) because positive and negative eigenfrequencies of equal magnitude are essentially identical. Equation (4) is also valid for the PT-symmetric system, as the eigenfrequencies in equation (4) are found to be independent of x. We note that if x=1, the PTX-symmetric system would degenerate into the PT one. The eigenmodes of the PT-symmetric system (Ψ'_k) and the PTX-symmetric system (Ψ'_k) can be written as:

$$\Psi'_{k} = c_{k} \left(e^{-i\phi' k}, e^{i\phi' k}, -i\omega_{k} e^{-i\phi' k}, -i\omega_{k} e^{i\phi' k} \right)^{T}, c_{k} \in \mathbb{R}$$
 (5a)

$$e^{2i\phi'k} = -\frac{\gamma \left[(1 - \kappa^2)\omega_k^2 - 1 \right] + i\omega_k}{\kappa(\gamma + i\omega_k)}$$
 (5b)

$$\Psi_k = \mathcal{S}^{-1} \Psi'_k \tag{5c}$$

Complex eigenfrequencies would evolve with γ , unveiling three distinct regimes of behaviour. The eigenfrequencies undergo a bifurcation process and branch out into the complex plane at the exceptional point (or spontaneous *PTX*-symmetry breaking point):

$$\gamma_{\rm EP} = \frac{1}{\kappa} \sqrt{\frac{1 + \sqrt{1 - \kappa^2}}{2}} \tag{6}$$

In the parametric region of interest $\gamma \in [\gamma_{EP}, \infty]$, PTX-symmetry is exact, rendering real eigenfrequencies and $PTXY_k = Y_k$. The region $\gamma \in [\gamma_c, \gamma_{EP}]$ is known as the broken PTX-symmetric phase with complex eigenfrequencies. Another crossing between the pairs of degenerate frequencies (and another branching) occurs at the lower critical point:

$$\gamma_{c} = \frac{1}{\kappa} \sqrt{\frac{1 - \sqrt{1 - \kappa^2}}{2}} \tag{7}$$

In the sub-critical region $\gamma \in [0, \gamma_c]$, ω_k become purely imaginary and, therefore, the modes have no oscillatory part and simply blow up or decay away exponentially. These modes correspond to the overdamped modes of a single oscillator, which is of little interest, particularly for sensor applications that require sharp resonances.

Wireless measurement set-ups. Our experimental set-up comprised a MEMSbased wireless pressure sensor, inductively coupled to a conventional passive reader or an active reader (a picture of the experimental set-up is shown in Supplementary Note 2). The MEMS varactor is constituted by two circular parallel metal sheets with a diameter of 4 mm and an air gap of 100 μm. To simulate variations of internal pressure inside the human eye, the sensor, placed on an XYZ linear translation stage, was encapsulated with epoxy polyamides and connected with an air compressor. A microprocessor-controlled regulator (SMC E/P Regulator) was used to control the internal pressure inside the air cavity of the MEMS varactor. The active reader composed of an -RLC tank was fixed and connected to a VNA (Agilent E5061B). This allows for precise control of the coupling strength κ between the MEMS-based pressure sensor and the reader coil. The internal pressure inside the micromachined air cavity of the sensor, as the main physiological parameter of interest, was characterized by tracking the resonance frequency from the measured reflection coefficients. In our experiments, the pressure was varied from 0 mmHg to 200 mmHg, and the VNA and the pressure regulator were synchronously controlled by the LabVIEW program.

Data availability. The data that support the plots within this paper and other findings of this study are available from the corresponding author upon reasonable request.

Received: 5 September 2017; Accepted: 12 April 2018; Published online: 14 May 2018

References

- Nopper, R., Niekrawietz, R. & Reindl, L. Wireless readout of passive LC sensors. IEEE Trans. Instrum. Meas. 59, 2450–2457 (2010).
- Collins, C. C. Miniature passive pressure transensor for implanting in the eye. IEEE Trans. Biomed. Eng. 2, 74–83 (1967).
- Pozar, D. M. Microwave Engineering 4th edn (John Wiley & Sons, New York, 2012).
- Mokwa, W. Medical implants based on microsystems. Meas. Sci. Technol. 18, R47–R57 (2007).
- Chavan, A. V. & Wise, K. D. Batch-processed vacuum-sealed capacitive pressure sensors. J. Micro. Syst. 10, 580–588 (2001).
- Chen, P. J., Rodger, D. C., Saati, S., Humayun, M. S. & Tai, Y. C. Microfabricated implantable parylene-based wireless passive intraocular pressure sensors. J. Micro. Syst. 17, 1342–1351 (2008).
- Chen, L. Y. et al. Continuous wireless pressure monitoring and mapping with ultra-small passive sensors for health monitoring and critical care. *Nat. Commun.* 5, 5028 (2014).
- Huang, H., Chen, P. Y., Hung, C. H., Gharpurey, R. & Akinwande, D. A zero power harmonic transponder sensor for ubiquitous wireless μL liquid-volume monitoring. Sci. Rep. 6, 18795 (2016).
- Yvanoff, M. & Venkataraman, J. A feasibility study of tissue characterization using LC sensors. IEEE Trans. Antenna Propagat. 57, 885–893 (2009).
- Bender, C. M. & Boettcher, S. Real spectra in non-Hermitian Hamiltonians having P T symmetry. *Phys. Rev. Lett.* 80, 5243 (1998).
- Makris, K. G., El-Ganainy, R., Christodoulides, D. N. & Musslimani, Z. H. Beam dynamics in PT symmetric optical lattices. *Phys. Rev. Lett.* 100, 103904 (2008).
- Rüter, Ch. E. et al. Observation of parity-time symmetry in optics. *Nat. Phys.* 192–195 (2010).
- Regensburger, A. et al. Parity-time synthetic photonic lattices. *Nature* 488, 167–171 (2012).
- Lin, Z. et al. Unidirectional invisibility induced by PT-symmetric periodic structures. *Phys. Rev. Lett.* 106, 213901 (2011).
- Mostafazadeh, A. Invisibility and PT symmetry. Phys. Rev. A 87, 012103 (2013).
- 16. Longhi, S. PT-symmetric laser absorber. Phys. Rev. A 82, 031801 (2010).
- Chong, Y. D., Ge, L. & Stone, A. D. PT-symmetry breaking and laserabsorber modes in optical scattering systems. *Phys. Rev. Lett.* 106, 093902 (2011).
- Feng, L., Wong, Z. J., Ma, R. M., Wang, Y. & Zhang, X. Single-mode laser by parity-time symmetry breaking. Science 346, 972–975 (2014).
- Hodaei, H., Miri, M. A., Heinrich, M., Christodoulides, D. N. & Khajavikhan, M. Parity-time-symmetric microring lasers. *Science* 346, 975–978 (2014).
- Wong, Z. J. et al. Lasing and anti-lasing in a single cavity. Nat. Photon. 10, 796–801 (2016).
- Lee, J. M. et al. Reconfigurable directional lasing modes in cavities with generalized PT symmetry. Phys. Rev. Lett. 112, 253902 (2014).
- Peng, B. et al. Parity-time-symmetric whispering-gallery microcavities. Nat. Phys. 10, 394–398 (2014).
- Ramezani, H., Kottos, T., El-Ganainy, R. & Christodoulides, D. N. Unidirectional nonlinear PT-symmetric optical structures. *Phys. Rev. A* 82, 043803 (2010).
- Chang, L. et al. Parity-time symmetry and variable optical isolation in active-passive-coupled microresonators. Nat. Photon. 8, 524–529 (2014).
- Schindler, J., Li, A., Zheng, M. C., Ellis, F. M. & Kottos, T. Experimental study of active LRC circuits with PT symmetries. *Phys. Rev. A* 84, 040101 (2011).
- 26. Schindler, J. et al. PT-symmetric electronics. J. Phys. A 45, 444029 (2012).
- Bender, N. et al. Observation of asymmetric transport in structures with active nonlinearities. *Phys. Rev. Lett.* 110, 234101 (2013).
- Fleury, R., Sounas, D. & Alù, A. An invisible acoustic sensor based on parity-time symmetry. Nat. Commun. 6, 5905 (2015).
- Lu, X. Y., Jing, H., Ma, J. Y. & Wu, Y. PT-symmetry-breaking chaos in optomechanics. *Phys. Rev. Lett.* 114, 253601 (2015).
- Xu, X. W., Liu, Y. X., Sun, C. P. & Li, Y. Mechanical PT symmetry in coupled optomechanical systems. *Phys. Rev. A* 92, 013852 (2015).
- Wiersig, J. Sensors operating at exceptional points: general theory. *Phys. Rev.* A 93, 033809 (2016).
- Chen, P. Y. & Jung, J. PT-symmetry and singularity-enhanced sensing based on photoexcited graphene metasurfaces. *Phys. Rev. Appl.* 5, 064018 (2016).
- Liu, Z. P. et al. Metrology with PT-symmetric cavities: enhanced sensitivity near the PT-phase transition. *Phys. Rev. Lett.* 117, 110802 (2016).
- Chen, W., Özdemir, Ş. K., Zhao, G., Wiersig, J. & Yang, L. Exceptional points enhance sensing in an optical microcavity. *Nature* 548, 192–196 (2017).
- Hodaei, H. et al. Enhanced sensitivity at higher-order exceptional points. Nature 548, 187–191 (2017).

Acknowledgements

This work has been supported by the NSF ECCS grant no. 1711409 (to P.-Y.C.), the Air Force Office of Scientific Research, the Welch Foundation with grant no. F-1802 (to A.A.) and the Army Research Office (ARO) grant no. W911NF-17-1-0481 (to R.E.-G.). Device fabrication was carried out in the Nano Fabrication Service Core (nFab) at the Wayne State University.

Author contributions

M.S., M.H. and Q.C. designed the *PT* and *PTX* circuits and performed experimental measurements. M.S., M.H., Q.C. and M.C. designed and fabricated the MEMS pressure sensor. P.-Y.C., M.S. and M.C. conceived the experimental concepts. P.-Y.C., M.C., R.E.-G. and A.A. developed the concepts. P.-Y.C. and A.A. planned and directed the research. P.-Y.C., R.E.G. and A.A. wrote the manuscript.

Competing interests

The authors declare no competing interests.

Additional information

 $\label{eq:supplementary} \textbf{Supplementary information} \ is \ available \ for this \ paper \ at \ https://doi.org/10.1038/s41928-018-0072-6.$

Reprints and permissions information is available at www.nature.com/reprints.

Correspondence and requests for materials should be addressed to P.-Y.C. or A.A.

Publisher's note: Springer Nature remains neutral with regard to jurisdictional claims in published maps and institutional affiliations.